**NURETH14-241** 

# TWO-PHASE SWIRLING FLOW IN A BARREL OF A STEAM SEPARATOR

Kenichi Katono<sup>1</sup>, Toshiki Matsubayashi<sup>2</sup>, Koji Nishida<sup>1</sup> and Akio Tomiyama<sup>2</sup>

Hitachi Ltd., Ibaraki, Japan

Kobe University, Kobe, Japan

#### Abstract

A downscaled model of a steam separator is used to understand characteristics of swirling flow after passing through the pick-off ring (POR). Main conclusions obtained are as follows. (1) At high liquid volume fluxes, many droplets entrain in the gas core at the downstream edge of the POR. The liquid film thickness above the POR gradually increases because many droplets deposit on the liquid film. (2) At low liquid volume fluxes, water accumulates just behind the POR. (3) Improvement of the POR, based on the model results, is effective for gas-liquid separation especially under high liquid volume flux conditions.

### Introduction

Boiling water reactors (BWRs) are equipped with steam separators for splitting a two-phase mixture into steam and water before feeding steam to the dryers and turbines. The steam separator consists of a standpipe, a diffuser with a swirler, and a barrel with several pick-off-rings (PORs). Stationary vanes of the swirler apply a large centrifugal force to the steam-water two-phase flow, and most of the water in the barrel rapidly migrates toward the barrel wall. An annular swirling flow with few droplets in the gas core is, therefore, formed in the barrel. The liquid film flow and the gas core flow are separated by the POR.

Sufficient information about the characteristics of two-phase swirling flow in the barrel is required for improving the separator performance. However, there is little available on annular swirling flow in the separator [1, 2]. Hence, in our previous studies [3, 4], we measured flow patterns, liquid film thickness, ratios of the separated liquid flow rate to the total liquid flow rate, and distributions of droplet diameter in air-water annular swirling flows from a diffuser to a barrel in a one-fifth scale model of the steam separator to understand the characteristics of the swirling flow and to establish an experimental database applicable to the modelling and verification of numerical methods for predicting the two-phase flow in the steam separator. We also experimentally examined the effects of POR shape [5] and swirler vane shape [6] on separation performance.

The purpose of the present study was to understand characteristics of swirling flow after passing through the POR. We did experiments at atmospheric pressure and room temperature using a downscaled model of the steam separator in which a simulated POR was installed. Flow patterns, liquid film thickness distribution and separation rate were measured for a wide range of gas and liquid volume fluxes to understand the effects of the simulated POR. We also designed an improved POR and examined its performance.

## 1. Experiments

## 1.1 Experimental setup

Figure 1 shows the experimental apparatus. It consisted of the upper tank, the barrel, the diffuser, the standpipe, the plenum, the gas-liquid mixing section, the water supply system and the air supply system. The barrel, diffuser and standpipe were made of transparent acrylic resin for observations and making optical measurements of two-phase flow. The size was about one-fifth of the actual steam separator for a BWR. Air was supplied to the mixing section from an oil-free compressor (Oil-free Scroll 11, Hitachi Ltd.), with control by a regulator (R600-20, CKD. Ltd.) and a flowmeter (FLT-N, Flowcell, Ltd.). Tap water at room temperature (293K) was supplied to the mixing section using a magnet pump (MD-40RX, Iwaki, Ltd.) with control by a flowmeter. The two-phase flow formed in the mixing section flowed up through the plenum (inner diameter D, 60 mm; length L, 300 mm), the standpipe (D = 30 mm; L = 200 mm), the diffuser (L = 33 mm), and the barrel (D = 40 mm; L = 240 mm).

Figure 2 shows a schematic of the flow pattern in the barrel. In an actual steam separator, the liquid film flow and the gas core flow are separated by the first POR and unseparated liquid, droplets and the gas flow into the second barrel. In this study, we installed the simulated POR in the barrel to simulate the flow condition around the first POR. The simulated POR had a sloping inlet to minimize the separation of liquid film at the inlet and the inner diameter at the simulated POR was 32 mm.

Figure 3 shows the upper part of the barrel, the upper tank and the device for separating the liquid film flow from the gas core flow, i.e. the mixture of gas and droplet flow. In an actual steam separator, the PORs are utilized for separation. An inner pipe was inserted in the upper part of the barrel to simulate the second POR. The lower end of the inner pipe was located 240 mm above the bottom of the barrel. The gap between the barrel wall and the outer wall of the inner pipe was 1.9 mm, and wall thickness and inner diameter of the inner pipe were 0.6 and 35.0 mm, respectively. Most of the liquid film flowed through the gap, while most of the air and droplets flowed through the inner pipe. The separated liquid and the droplets carried over were returned to the water reservoir through independent pipelines.

# 1.2 Experimental conditions and measurements

Experimental conditions were determined by adjusting the values of the flow quality and two-phase centrifugal force to cover those in the nominal operating conditions of the BWR separator. The values of the flow quality x, the gas and liquid volume fluxes in the barrel,  $J_G$  and  $J_L$ , corresponding to the nominal operating conditions of the Hyper ABWR [7] are 0.18, 14.6 m/s, and 0.080 m/s, respectively [3]. Liquid volume flux that passes through the first POR and flows into the second barrel is lower than that in the first barrel because liquid film in the first barrel is mostly separated by the first POR. Hence, the present experiments were carried out under the conditions of  $J_G = 8.0 - 24.1$  m/s and  $J_L = 0.005 - 0.080$  m/s.

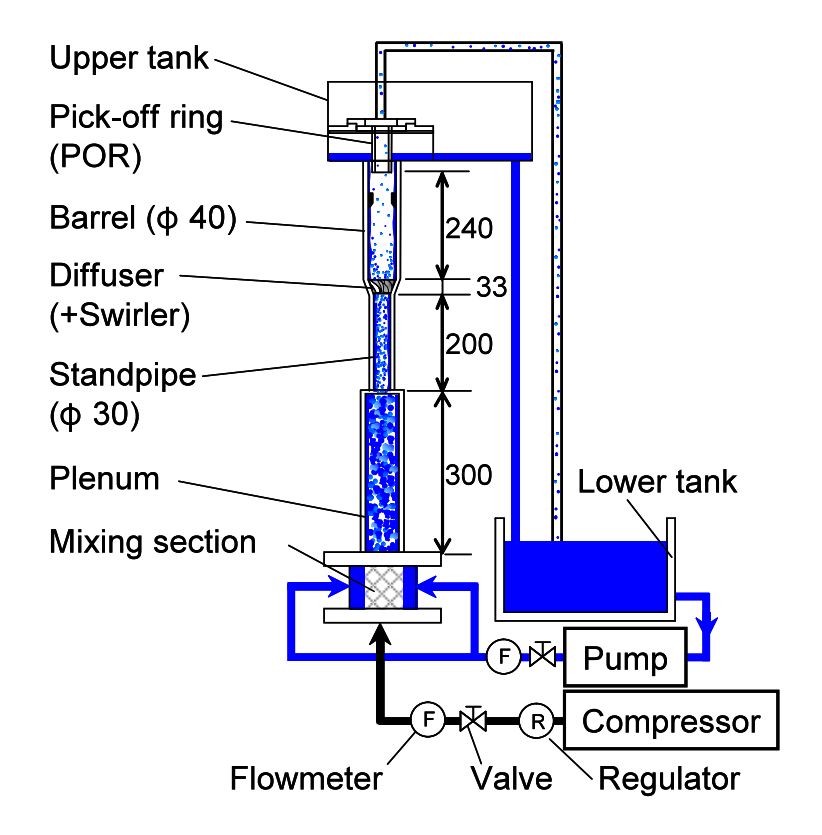


Figure 1 Experimental setup.

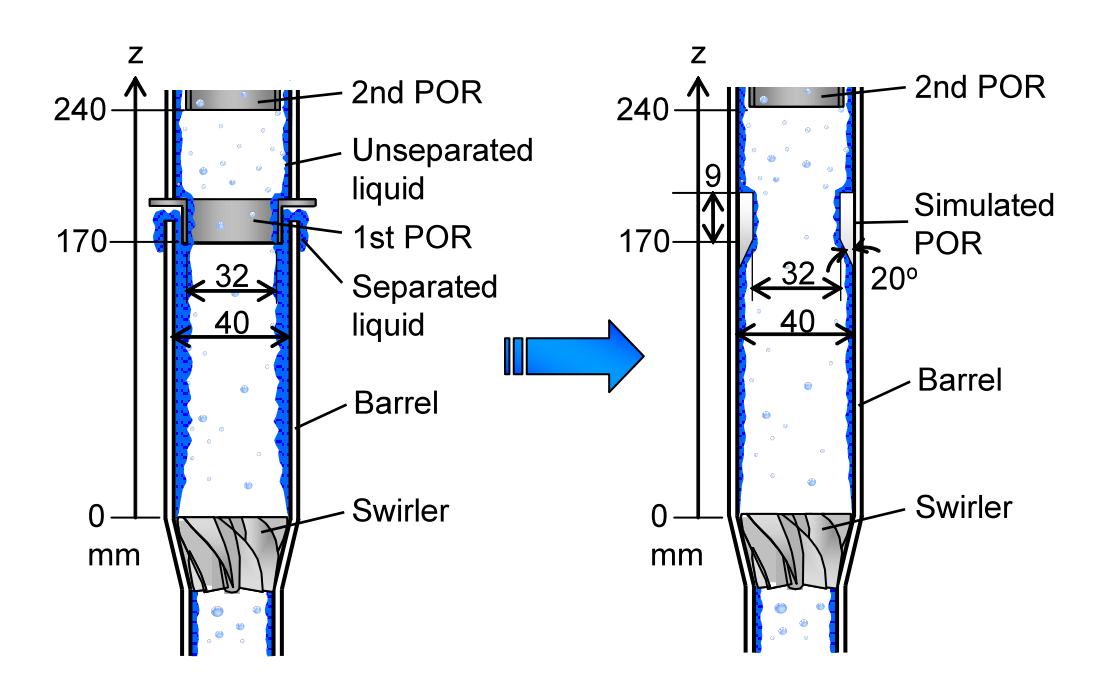


Figure 2 Schematic of flow pattern in the barrel.

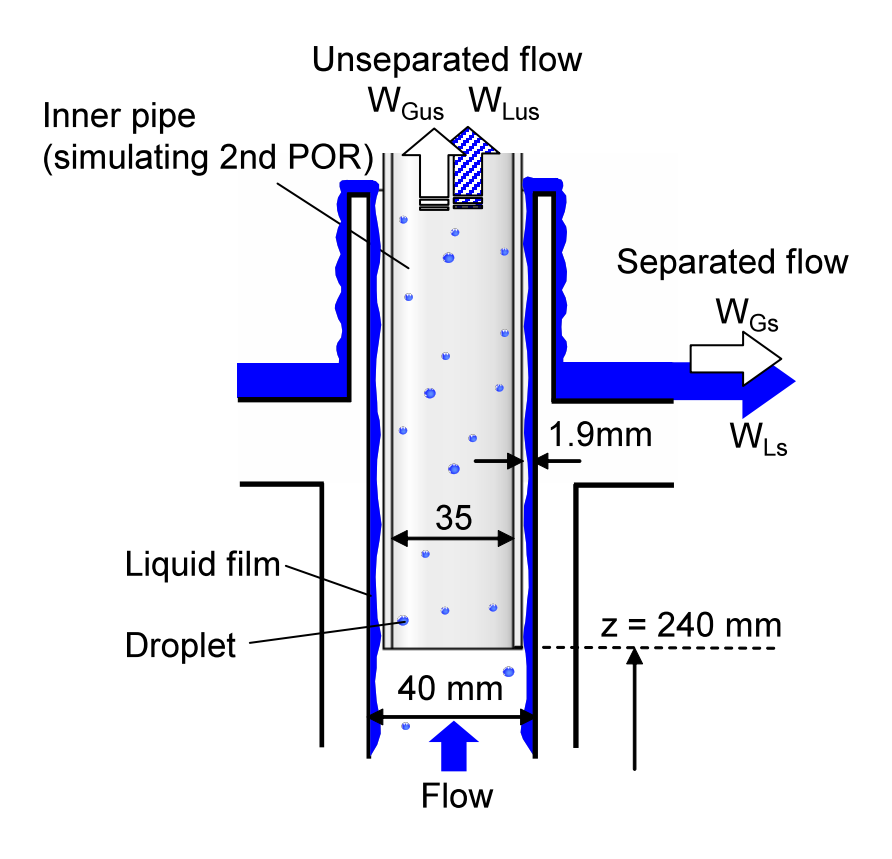


Figure 3 Separation part.

Flow patterns in the barrel were observed using a high-speed video camera (Redlake Motion Pro HS-1, frame rate = 4000 frame/s, exposure time = 100  $\mu$ s). The mass flow rates  $W_{Ls}$  and  $W_{Lus}$  of the separated liquid and the unseparated liquid returning to the reservoir were measured using a timer and graduated cylinders. Each measurement was conducted for 50 s to make the uncertainty estimated at the 95% confidence interval in measured flow rates less than 3%. The ratio  $W_s$ \* of the separated flow rate to the total liquid flow rate was used as an index of the separator performance and is defined by Eq. (1).

$$W_s^* = \frac{W_{Ls}}{W_{Ls} + W_{Lus}} \tag{1}$$

The film thickness  $\delta$  was measured using a laser focus displacement meter (LFD, LT-9030, Keyence, Ltd.) [8]. The sampling period was 0.64 ms and the measurement time was 32 s. Hence the sampling number was 50,000 points, which was a large enough number to obtain an accurate time-averaged film thickness  $\delta_{mean}$ . The uncertainty in measured  $\delta$  was 0.65% [9].

#### 2. Results and discussion

### 2.1 Flow visualization

Recorded images of flow patterns at  $J_L = 0.080$  m/s are shown in Fig. 4. The flow pattern transited from churn to annular flows as  $J_G$  increased. Under the churn flow conditions, the liquid film sometimes fell along the barrel wall, whereas under the annular flow conditions the film continuously flowed upward. At the annular flow condition ( $J_G = 14.6$ , 24.1 m/s), the liquid film separated at the downstream edge of the simulated POR, and the separation area increased with increasing  $J_G$ . Some of the separated liquid film was entrained as droplets in the gas core flow and the rest of the separated liquid film was attached to the barrel wall as the liquid film. And the droplet deposition took place in the barrel above the simulated POR.

Recorded image of flow patterns at  $J_G = 14.6$  m/s are shown in Fig. 5. In an actual steam separator, liquid volume flux in the second barrel is lower than that in the first barrel. The liquid film separation area decreased with decreasing  $J_L$  and water accumulated just behind the simulated POR.

Figure 6 shows the inner barrel flow patterns which were recorded using a bore scope (R080-084-000-50, Olympus Corp.) mounted on a high-speed video camera. At high liquid volume flux,  $J_L = 0.065$  m/s, a large amount of droplets entrained behind the simulated POR, while the amount of droplets in the barrel decreased with increasing  $J_G$ . This was because the amount of droplet deposition on the liquid film increased due to the large centrifugal force with increasing  $J_G$ . In contrast, at low liquid volume flux,  $J_L = 0.005$  m/s, only a few droplets were present in the gas core flow. Under all flow rate conditions in this study, we confirmed that there remained the centrifugal force in the barrel above the simulated POR.

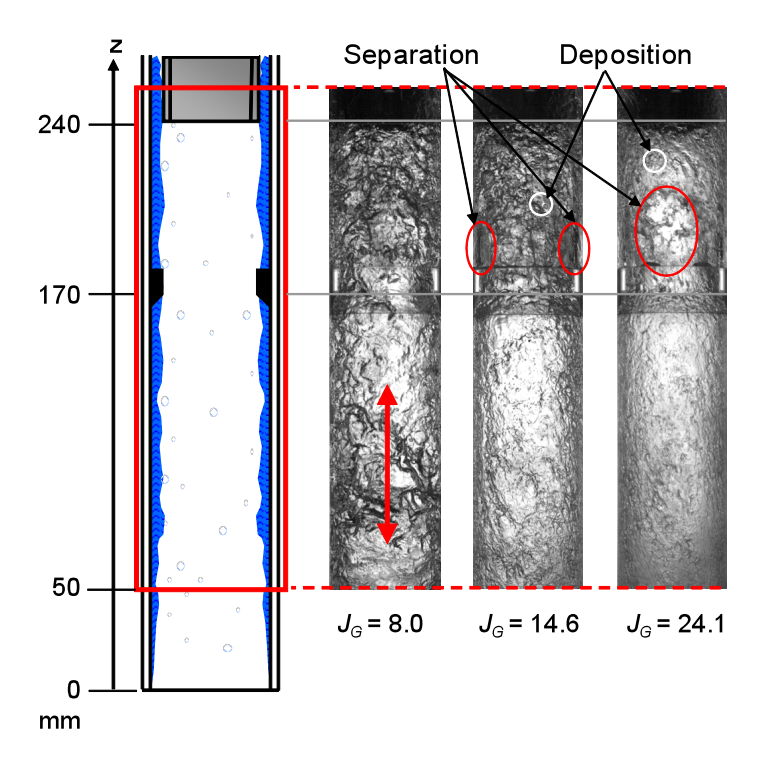


Figure 4 Flow pattern in the barrel ( $J_L = 0.080 \text{ m/s}$ ).

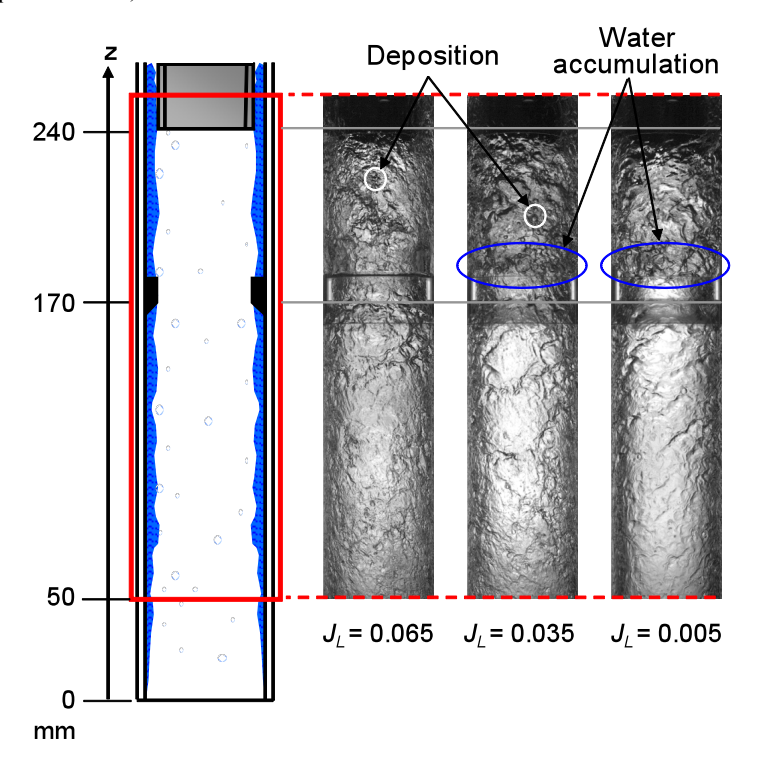


Figure 5 Flow pattern in the barrel ( $J_G = 14.6 \text{ m/s}$ ).

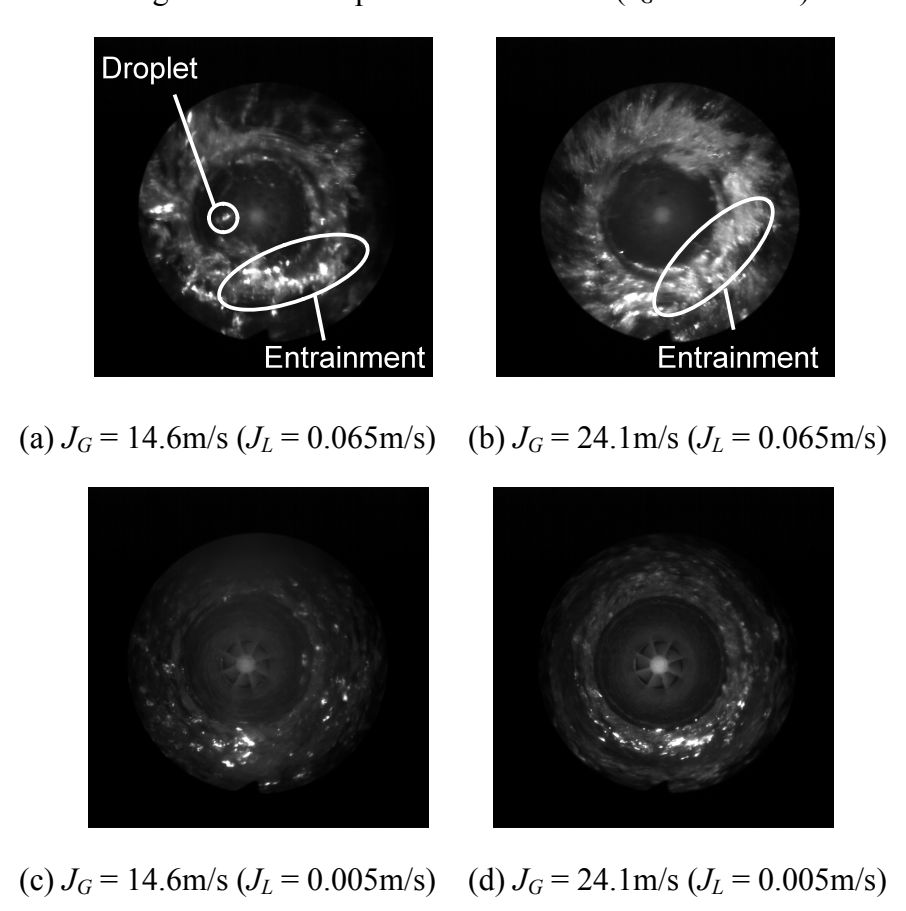


Figure 6 Inner barrel flow pattern (z = 240 mm).

#### 2.2 Film thickness

The mean film thickness  $\delta_{mean}$  was defined as the arithmetic average of measured instantaneous film thickness  $\delta$ . The maximum film thickness  $\delta_{max}$  was defined as the value of film thickness for which the cumulative probability distribution of film thickness was 99 %.

Figure 7 shows the liquid film thickness distributions in the barrel without an inner pipe under the condition of  $J_G = 14.6$  m/s. At low liquid volume fluxes ( $J_L = 0.005 - 0.035$  m/s), liquid film thickness was thick closer to the expansion part of the barrel and gradually decreased in the flow direction. As shown in Fig. 8 (a), water accumulated just behind the simulated POR and the amount of droplet entrainment was low at the downstream edge of the simulated POR. In the barrel above the simulated POR, liquid film was stretched due to the interfacial shear force.

Under high liquid volume flux conditions ( $J_L = 0.065$ , 0.080 m/s), the liquid film thickness above the simulated POR gradually increased. Although the liquid film separated and many droplets entrained in the gas core at the downstream edge of the simulated POR, droplets deposited on the liquid film by centrifugal force were still large enough to move droplets in the barrel above the simulated POR (Fig. 8 (b)).

The liquid film thickness around the expansion part of the barrel decreased with increasing  $J_L$ . This meant that the amount of the droplet entrainment at the downstream edge of the simulated POR increased with increasing  $J_L$ .

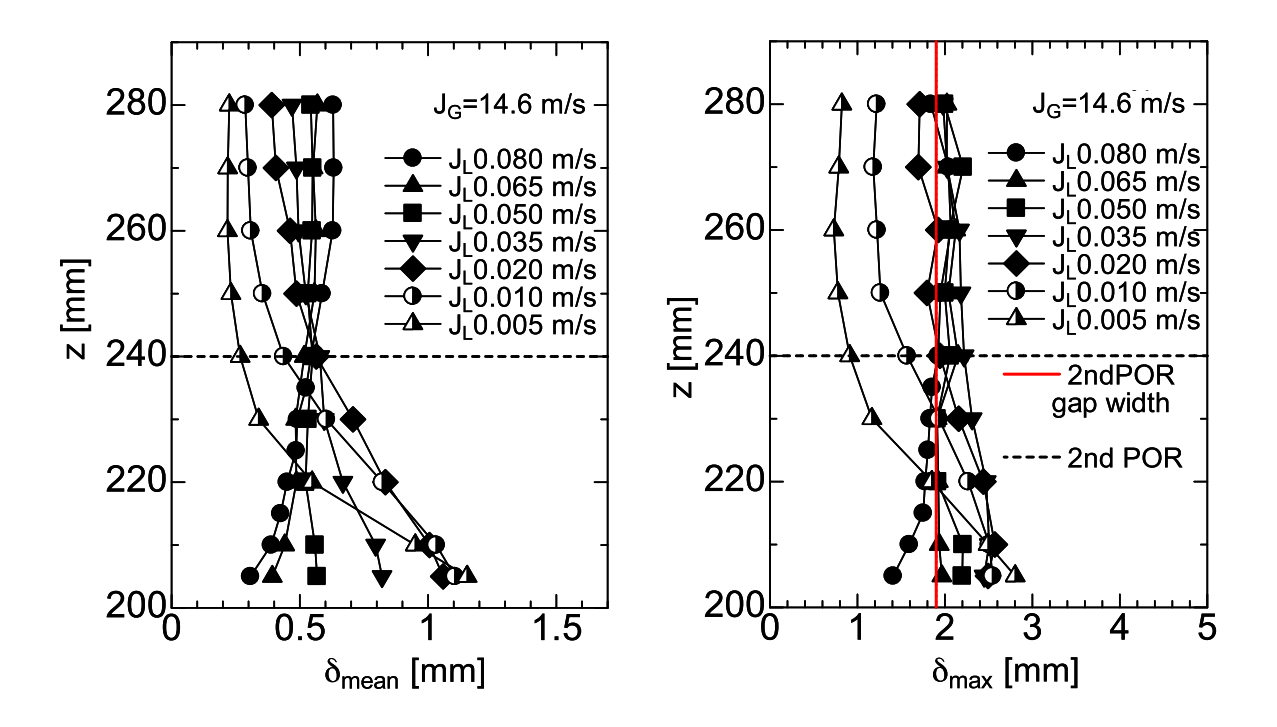
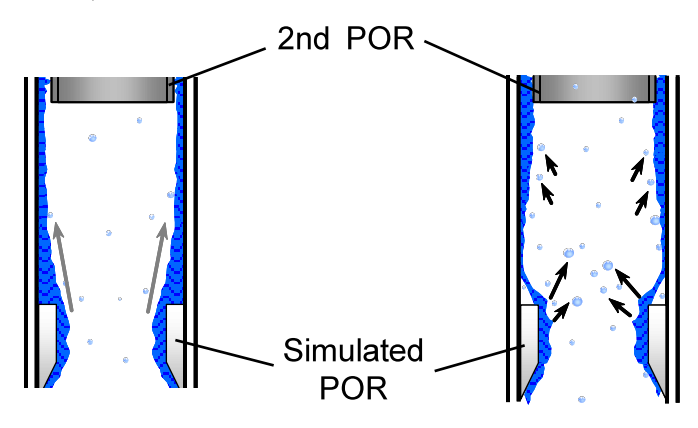


Figure 7 Liquid film thickness distributions ( $J_G = 14.6 \text{ m/s}$ ).



- (a) Low liquid volume flux case
- (b) High liquid volume flux case

Figure 8 Schematic of flow pattern around the simulated POR.

Figure 9 shows the effects of  $J_G$  on liquid film thickness distribution at  $J_L = 0.080$  m/s. The liquid film thickness decreased with increasing  $J_G$ . This was clearly due to the increase in the interfacial friction. The collar vertical lines in Fig. 9 show the mean liquid film thickness at the position of the first POR without the simulated POR,  $(\delta_{mean})_{first}$ . The difference between  $(\delta_{mean})_{first}$  and  $\delta_{mean}$  in the position of the second POR (z = 240 mm) decreased with increasing  $J_G$ . This was because centrifugal force in the barrel above the simulated POR increased with increasing  $J_G$ , so the amount of droplet deposition on the liquid film increased.

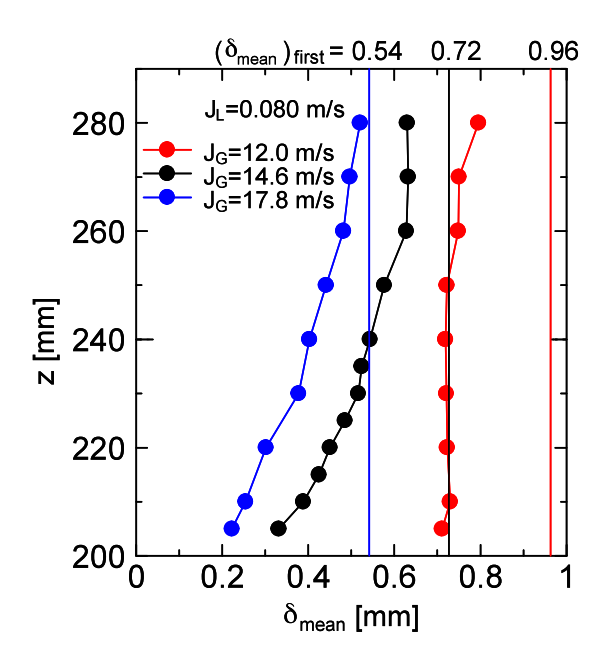


Figure 9 Effects of  $J_G$  on liquid film thickness distribution ( $J_L = 0.080 \text{ m/s}$ ).

#### 2.3 Flow separation

Figure 10 shows the measured  $W_s^*$ . At high liquid volume fluxes ( $J_L = 0.035 - 0.065$  m/s) and low gas volume fluxes ( $J_G = 12.0 - 17.8$  m/s), the difference of  $J_L$  had little effect on  $W_s^*$ . This was because the maximum liquid film thickness  $\delta_{\text{max}}$  was larger than the gap width between the second POR and the barrel wall as shown in Fig. 7. In contrast, the difference of  $J_L$  had an effect on  $W_s^*$  at high gas volume fluxes ( $J_G > 21.0$  m/s). At high gas volume fluxes, a large amount of droplets was entrained at the simulated POR by the gas core flow. So at high liquid volume fluxes, many droplets were not deposited on the liquid film and still existed at the position of the second POR. Hence,  $W_s^*$  was small at higher liquid volume fluxes.

At low liquid volume fluxes ( $J_L = 0.005$ , 0.010 m/s),  $W_s$ \* was higher than that at the high liquid volume fluxes. This was because the maximum liquid film thickness  $\delta_{\text{max}}$  was smaller than the gap width between the second POR and the barrel wall. In particular, at  $J_G = 17.8 - 24.1$  m/s and  $J_L = 0.005$  m/s,  $W_s$ \* was 1.0. These results meant that no droplets existed in the gas core flow. These results were consistent with the flow pattern at  $J_G = 24.1$  m/s and  $J_L = 0.005$  m/s as shown in Fig. 6 (d).

 $W_s$ \* at  $J_L = 0.020$  m/s was higher than that at  $J_L = 0.035 - 0.065$  m/s, although the maximum liquid film thickness  $\delta_{\text{max}}$  at  $J_L = 0.020$  m/s was about the same. This was because the passage frequency of the disturbance wave which travelled on the liquid film was low.

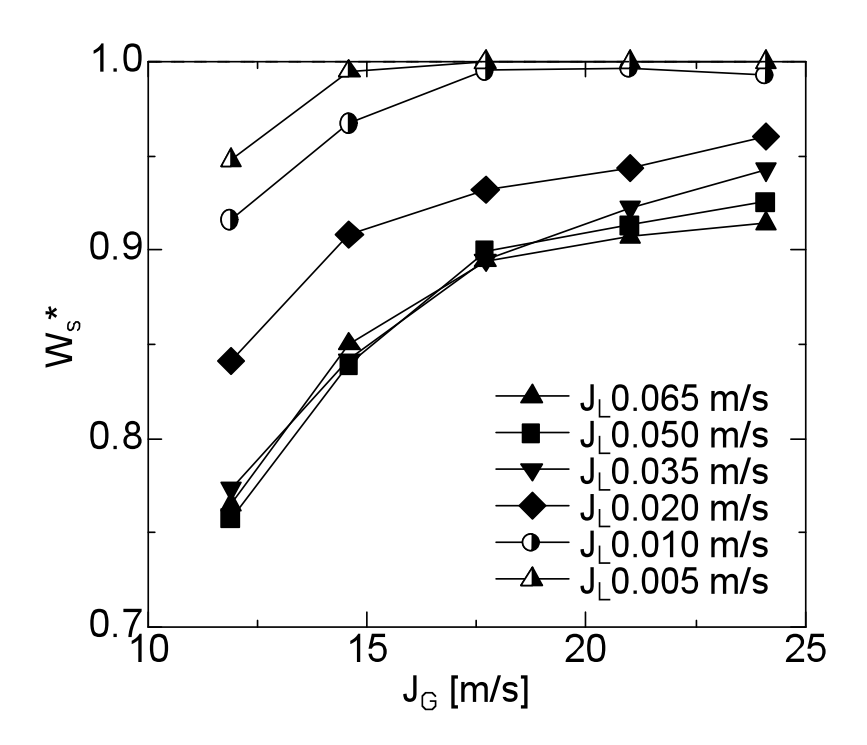


Figure 10 Effects of  $J_L$  on  $W_s^*$ .

## 3. Improvement of POR

In the previous section, we confirmed that the droplet entrainment was large at the sudden expansion part of the simulated POR exit, especially under the high liquid volume flux conditions. The separation performance of the second POR was degraded due to the droplet entrainment. In this study, an improved simulated POR, which had a sloping tail to minimize separation of the liquid film at the tail (shown Fig. 11), was installed and its performance was examined. The angle of the sloping tail was determined based on the diffuser performance curve for the single phase flow [10].

Figure 12 shows measured  $W_s^*$  of the normal POR and the improved simulated POR. At high liquid volume fluxes ( $J_L = 0.020 - 0.065$  m/s), the improvement effect on the liquid separation performance was large. In contrast, at low liquid volume fluxes ( $J_L = 0.005$ , 0.010 m/s), the improved POR had only a small effect on  $W_s^*$  because the amount of the droplet entrainment originally was small. For all flow rate conditions in this study, we confirmed that the suppression of the droplet entrainment by the improved simulated POR was effective.

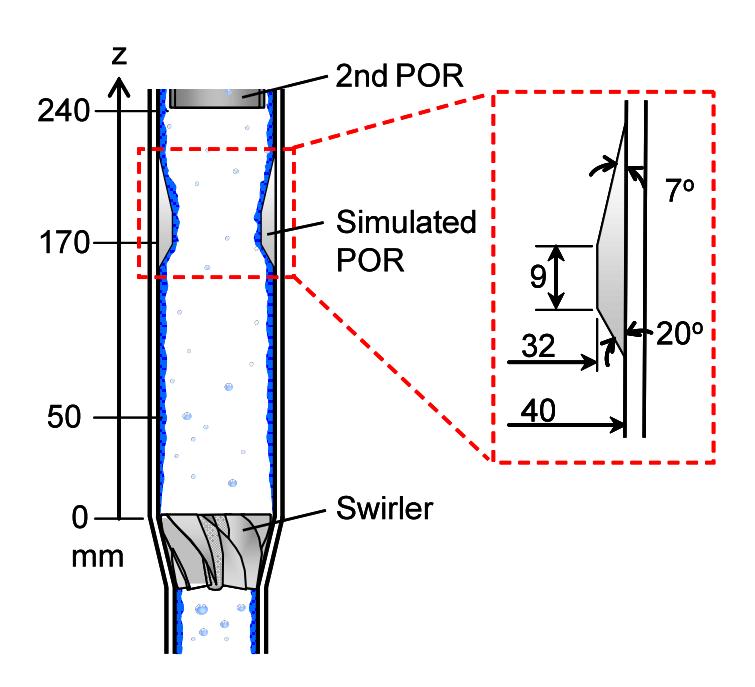


Figure 11 Improved simulated POR.

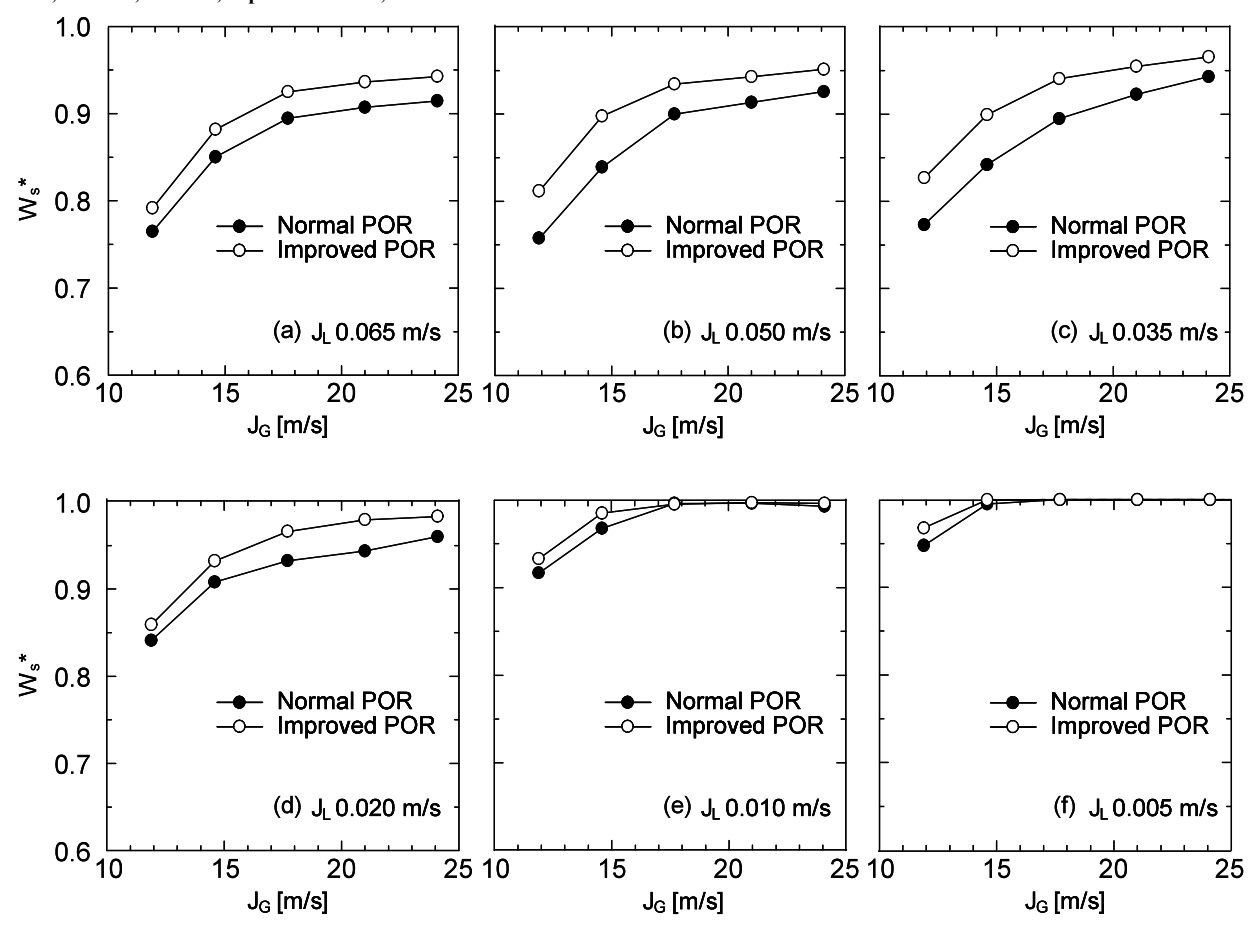


Figure 12 Effects of POR shape on  $W_s^*$ .

### 4. Conclusion

The characteristics of swirling flow after passing through the POR was experimentally investigated using a downscaled model of the steam separator in which a simulated POR was installed. Flow patterns, liquid film thickness distribution and separation rate were measured using a high-speed camera, a laser focus displacement meter and flowmeters. An improved POR, which had a sloping tail for minimizing the separation of liquid film at the tail, was installed and its performance was examined. As a result, the following conclusions were obtained.

- (1) At high liquid volume fluxes, the liquid film separated and many droplets were entrained in the gas core at the downstream edge of the simulated POR. The liquid film thickness above the POR gradually increased because many droplets deposited on the liquid film by centrifugal force still large enough to move droplets.
- (2) At low liquid volume fluxes, water accumulated just behind the simulated POR, and the film thickness decreased in the flow direction due to the interfacial shear force.
- (3) The improved POR was effective for gas-liquid separation especially under high liquid volume fluxes because the amount of the droplets formed at the POR was low at high liquid flow rates.

# 5. References

- [1] T. Nakao, M. Murase, N. Ishida, T. Kawamura, A. Minato and K. Moriya, "Decrease of pressure loss in BWR steam separator (1) (Evaluation method of gas-liquid separation)", *Japanese Journal of Multiphase Flow*, Vol. 15, No. 4, 2001, pp. 382-389. (In Japanese.)
- [2] H. Ikeda, T. Shimizu, T. Narabayashi, T. Kondo, K. Nishida and T. Fukuda, "Improvement of BWR steam separator with three-dimensional gas-liquid two-phase flow simulation method", <u>Proceedings of the 11th International Conference on Nuclear Engineering (ICONE-11)</u>, Paper No. 36486, 2003, pp. 1-9.
- [3] H. Kataoka, A. Tomiyama, S. Hosokawa, A. Sou and M. Chaki, "Two-phase swirling Flow in a gas-liquid separator", *Journal of Power and Energy Systems*, Vol. 2, No. 4, 2008, pp. 1120-1131.
- [4] H. Kataoka, A. Tomiyama, S. Hosokawa, A. Sou and M. Chaki, "Swirling annular flow in a steam separator", *Journal of Engineering of Gas Turbines and Power*, Vol. 131, Paper No. 032904, 2009, pp. 1-7.
- [5] H. Kataoka, A. Tomiyama, S. Hosokawa, A. Sou and M. Chaki, "Effects of pick-off-ring configuration on separation performance of gas-liquid separator", Progress in Multiphase Flow Research, 2007, pp. 67-74. (In Japanese.)
- [6] H. Kataoka, Y. Shinkai and A. Tomiyama, "Effects of swirler shape on two-phase swirling flow in a steam separator", *Journal of Power and Energy Systems*, Vol. 3, No. 2, 2009, pp. 347-355.
- [7] K. Mishima, A. Tomiyama, T. Okawa, H. Takeuchi, Y. Kudo, Y. Yamamoto and M. Chaki, "Research on ABWR plants of hyper core power density", <u>Proceedings of the 11th National Symposium on Power and Energy Systems (SPES 2006)</u>, Vol. 11, 2006, pp. 225-230. *in Japanese*.
- [8] T. Takamasa and T. Hazuku, "Measuring a film flowing down a vertical wall using laser focus displacement meters (1st Report, measuring principle and film thickness)", *Transactions of the Japan Society of Mechanical Engineers, Series B*, Vol. 64, No. 617, 1998, pp. 128-135. (In Japanese.)
- [9] H. Kataoka, Y. Shinkai and A. Tomiyama, "Pressure Drop in Two-Phase Swirling Flow in a Steam Separator", *Journal of Power and Energy Systems*, Vol. 3, No. 2, 2009, pp. 382-392.
- [10] JSME Data Book, Hydraulic Losses in Pipes and Ducts, 1993. (In Japanese.)